# Novel optical detection system for *in vivo* identification and localization of cervical intraepithelial neoplasia

**Kevin T. Schomacker**
**Thomas M. Meese**
**Chunsheng Jiang**
**Charles C. Abele**
**Karen Dickson**
**Stephen T. Sum**
**Ross F. Flewelling**
MediSpectra, Incorporated
45 Hartwell Avenue
Lexington, Massachusetts 02421

**Abstract.** A noncontact optical detection system is developed for the *in vivo* identification and localization of high-grade cervical intraepithelial neoplasia (CIN 2,3). Diagnostic scans of the entire human cervix are performed following acetic acid application employing three integrated optical measurements: laser-induced fluorescence spectroscopy, white light diffuse reflectance spectroscopy, and video imaging. Full cervical scans comprising 499 interrogation locations at 1-mm spatial resolution are completed in 12 s. Diffuse reflectance and fluorescence spectra with signal-to-noise ratios of better than 100-to-1 are collected between 360 and 720 nm in increments of 1 nm, with an inherent spectral resolution of 8 nm. Glare reduction and optical vignetting are handled with a novel illumination scheme and subsequent spectral arbitration algorithms. The system is designed and found to be well below acceptable safe optical exposure levels. Typical reproducibility across multiple systems is approximately 5%, providing reliable and accurate detection of *in vivo* cervical neoplasia in normal clinical use. 
[DOI: 10.1117/1.2208987]

Keywords: fluorescence; diffuse reflectance; colposcopy; calibration; glare reduction; UV safety analysis.

Paper 05220R received Jul. 29, 2005; revised manuscript received Jan. 19, 2006; accepted for publication Feb. 15, 2006; published online Jun. 6, 2006.

## 1 Introduction

Cervical cancer prevention in the United States is based on routine cervical cytologic (Pap) screening, followed by triage of abnormal cytology findings. The American Society for Colposcopy and Cervical Pathology consensus guidelines recommend colposcopy for women with low-grade squamous intraepithelial lesions (LSIL) or higher, and for women with atypical squamous cells of undetermined significance (ASCUS) who have tested positive for high-risk human papillomavirus (HPV) strains or have repeat ASCUS cytology.[1] As a consequence, approximately 1 to 1.25 million women with LSIL cytology findings and 1 to 1.5 million women with ASCUS cytology findings are referred each year to follow-up colposcopy.[2] The purpose of colposcopy is to identify areas of the cervix suspicious for high-grade cervical intraepithelial neoplasia (CIN 2,3) and to take a representative biopsy of those areas for pathological evaluation. Women found positive are then referred on for appropriate treatment.

The sensitivity for detecting CIN 2,3 at colposcopy is estimated to be 64% for women with ASCUS cytology results[3] and 67% for women with LSIL cytology results,[4] based on the number of women with CIN 2,3 lesions found at initial colposcopy compared to the cumulative number found over aggressive two-year follow-up. When these data were projected to the colposcopy referral population, it was estimated that approximately one third of high-grade disease was missed by initial colposcopy.[2] Given that some 500,000 cases of CIN 2,3 are found each year,[1] missing approximately one third of the disease means that approximately 165,000 cases of high-grade disease may go undetected at colposcopy.

Quantitative optical spectroscopy has now developed to the point where precommercial systems are under clinical evaluation as aids to colposcopy for the safe and reliable detection of intraepithelial neoplasia of the uterine cervix. Several recent review articles have reported on the various approaches being pursued.[5–8] In the largest clinical evaluation of its kind, an optical detection system (ODS) was trained and evaluated on 604 patients with the finding that as much as a 33% increase in the detection of CIN 2,3 was possible as compared to colposcopy alone.[9] The purpose of this work is to describe in detail the design and performance characteristics of this novel ODS, including an assessment of the calibration, stability, and human safety of the system.

## 2 Materials and Methods

### 2.1 *System Modules and Spectral Subsystems*

The ODS design consists of three main components: a console, an optical probe head, and a single-use sheath (Fig. 1). The console contains all of the light sources, coupling optics, spectrometer, and electronics, and includes a calibration port for probe calibration prior to each patient scan. The optical probe is interfaced to the console by way of an articulating arm that supports the electrical and optical cables. A single-

Address all correspondence to Kevin Schomacker, HyperMed, Inc., 305 Second Avenue-Suite B, Waltham, MA 02451 United States of America; Tel: 781-487-0545; Fax: 781-487-4199; E-mail: kschomacker@comcast.net

1083-3668/2006/11(3)/034009/12/$22.00 © 2006 SPIE

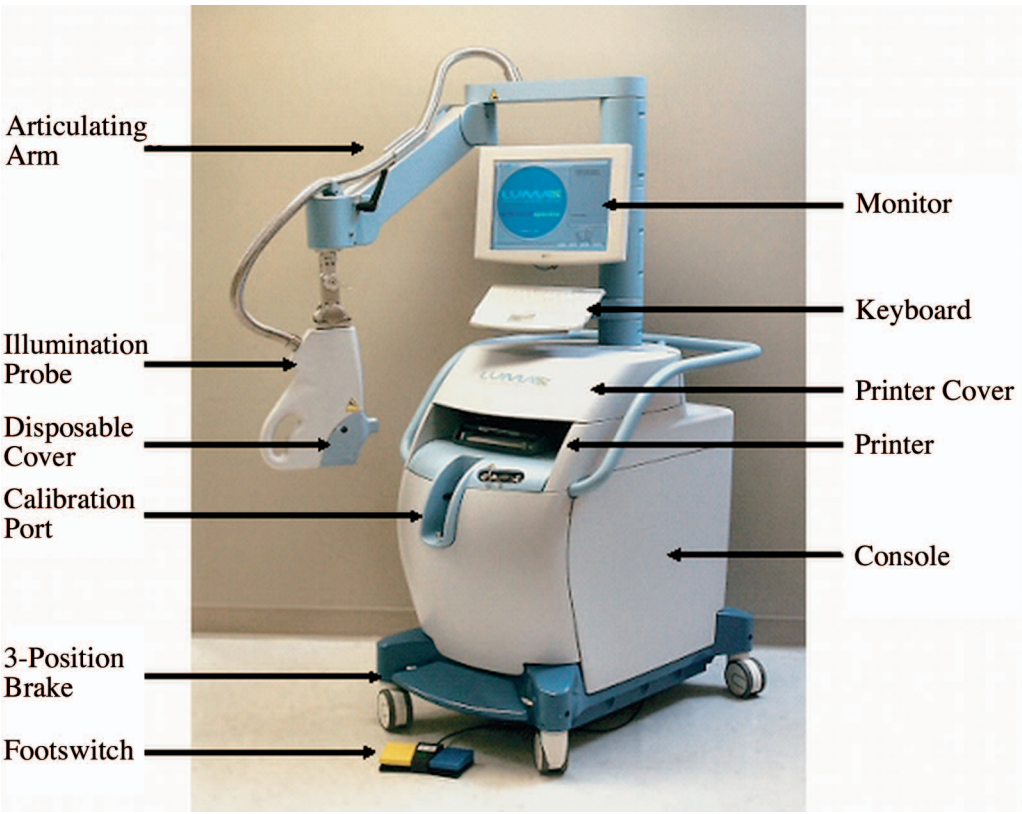


**Fig. 1** Photograph of the optical detection system showing some major features.

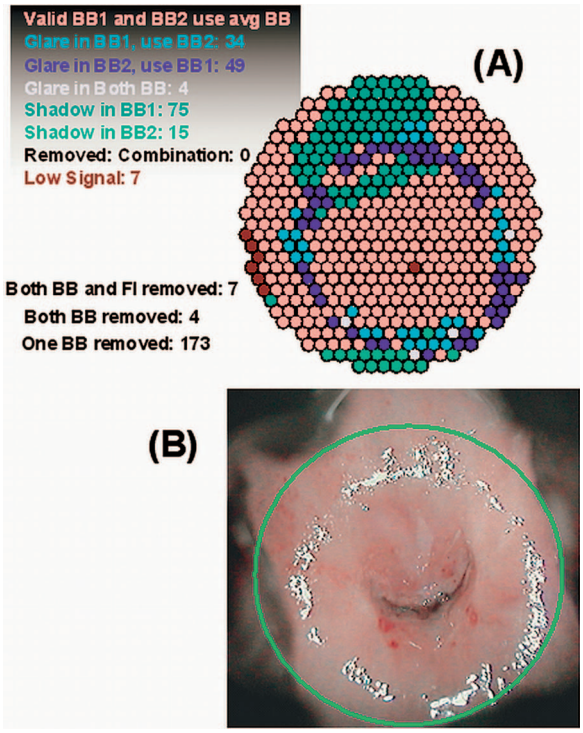


**Fig. 3** Graphical representation of the spectral arbitration routines. (a) For this subject, only four measurement sites were lost due to glare being present in BB1 and BB2 (light gray circles), even though 173 sites were identified with glare or shadow in at least one channel. Combination includes sites with glare and shadow. (b) White light image of cervix showing the area scanned in (a) and includes a ring of glare.

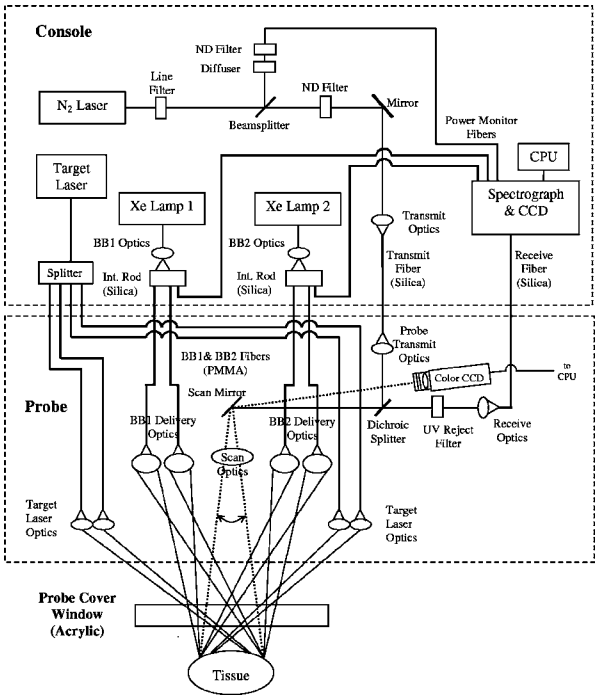


**Fig. 2** Schematic of optical detection system.

use sheath snaps onto the optical probe and protects the patient and the optics against cross-contamination. In use, the optical probe is positioned near the yolk of a vaginal speculum to view the cervix. The system is operated using custom software running on an embedded computer. The user interacts with the computer through a keyboard, a touch pad, and a dual-element foot pedal. The final system output is a video image of the cervix with a false-color overlay indicating areas of suspected high-grade disease.

The spectral subsystems include the UV source, the broadband source, their respective coupling optics, the spectrometer and detector, the calibration system, the probe optics, the scanner assembly, the broadband illuminator, and the sheath. A detailed breakdown of the optical paths is shown in Fig. 2. The transmit path for the UV source and the broadband sources differ. The UV source is used to induce tissue fluorescence, while the broadband source is used to measure diffuse reflectance. The spectrometer, detector, probe collection optics, and sheath window are common for fluorescence and diffuse reflectance measurements.

The UV source is used to induce fluorescence from the cervix and other calibration targets. Light from a pulsed nitrogen laser (model 337201-99, Spectra-Physics, Mountain View, California; 200-$\mu$J nominal power output; 4.5 ns pulse width) is passed through a 337-nm laser line filter, then shunted by a beamsplitter, sending 5% of the beam through a 60-deg holographic diffuser into a UV-transmitting fiber directing laser energy onto one end of a 532-channel charge-coupled device (CCD) detector (S7031-0906, Hamamatsu Corporation, Bridgewater, New Jersey) (the CCD is split into spectral and energy-monitoring sections). The energy in this leg is used to monitor the laser energy and to correct for pulse-to-pulse energy fluctuations. Neutral density filters are used to control the energy on the detector in the energy-monitor beam and in the excitation beam delivered to tissue. The system is designed to deliver to tissue between 16 and 35 $\mu$J per pulse of 337-nm light.

The primary beam is coupled into a tapered 0.4- to 0.2-mm core, 0.22-NA optical fiber that delivers the light to a set of collimating optics in the probe head. After reflecting off a dichroic beamsplitter and a 2-D galvo-driven stepping mirror (M3 Series, GSI Lumonics Incorporated), the beam is passed through a set of scan lenses designed to focus the beam to an in-focus diameter of 0.8 mm on the cervix. The scan lenses included a three lens system designed to have minimal chromatic and spherical aberrations between 330 and 720 nm and used low fluorescence I-line glass and antireflective coatings. The distance between the last lens and the focal plane is 130 mm. The scan mirror raster scans a 25-mm-diam circular region on the cervix by stepping back and forth through 499 individual, hexagonal-packed sites having a 1.1-mm center-to-center distance between adjacent sites. 25 lines having varying number of measurement steps cover the 25-mm-diam circular region [see Fig. 3(a)].

Diffuse reflectance spectra are collected concurrently with the fluorescence data. Light from two 20-W xenon flashlamps (FX-1160, Perkin Elmer, Salem, Massachusetts) is coupled into separate optically integrating rods, and then each rod splits the light among three emergent fibers. The first fiber of each integrating rod delivers about 5% of the light to the CCD/spectrograph for energy monitoring. The rest of the light in each rod is split between two broadband fibers (PGR-FB2000, Toray Plastics, New York, 4.3 m in length) that deliver the light to the probe head. Thus, a total of four broadband transmit fibers (two from each of the rods) delivers light to four projection lenses that alternately flood illuminate the cervix from two angles (either from two upper sources or from two lower sources). The effective illumination area is 3.2 cm in diameter. The broadband emission spectrum is maximal at 487 nm and drops to about 10% of the peak at both 360 and 720 nm. Absorption occurring in the broadband transmit fibers and optics strongly attenuates light below 320 nm. The broadband energy incident onto tissue is set to approximately 300 $\mu$J (range 290 to 310 $\mu$J).

The diffuse reflectance and fluorescence emission from cervical tissue are collected by the same scan lenses, passed through a dichroic beamsplitter and a 337-nm excitation rejection filter, and then focused by the receive optics into a 0.2-mm core, 0.22-NA receive fiber. The receive fiber transmits the signal directly to the input of a broadband spectrograph (CP140-3301, Jobin Yvon OEM Group, Edison, New Jersey), which disperses the light onto the spectral portion of the CCD. Spectra are recorded between 360 and 720 nm at approximately 1-nm resolution.

The ODS scans the cervix by collecting one fluorescence spectrum, two diffuse reflectance spectra (using the upper and lower light sources), and one background spectrum at each tissue measurement site. The background signal is measured within the same detector cycle. One detector cycle consists of five 3.3-ms periods corresponding to a clear-detector period, a background measurement, the diffuse reflectance measurement with the upper lamps, the diffuse reflectance measurement with the lower lamps, and finally the fluorescence measurement. All detector measurements include a spectral region

(CCD bins 11 to 401) and an energy-monitoring region (CCD bins 402 to 522). The 2-D detector dimension is 64 (imaging axis) by 532 (spectral axis) pixels. The imaging axis is summed into single bins.

### 2.2 *Calibration System*

A full system calibration is performed routinely during system build and maintenance procedures using internal and external calibration targets and procedures. External targets include the use of a reference fluorescence dye cell, a calibrated nominal 60% diffuse reflectance target, and additional specialized video targets. The fluorescence intensity of the dye cell is a controlled reference that is used to correct across systems for the inherent differences in the collection efficiency of the different systems. The 60% target is used as an across-system reference for the diffuse reflectance measurement. The video targets consist of a split 10/20% diffuse reflectance target that is used to adjust the contrast and gain on the video camera, and a color target that is used to adjust the color balance.

Additional calibration sources include the use of argon and mercury pen lamps and a calibrated tungsten-halogen lamp. Internal targets and sources include a null target, a nominal 10% diffuse reflectance target, a small frequency doubled Nd:YAG pen laser, a pulsed nitrogen laser, and two pulsed xenon lamps. The use of all targets and sources are described in more detail later.

In addition to routine full system calibration, additional run-time calibration procedures are made to check for changes that may occur between full system calibrations. Small changes are accounted for in the calibration procedures, while large changes prevent the user from proceeding to patient measurements. Run-time calibration is done just with the internal targets and sources. The number of calibration checks and targets are intentionally limited to improve the reliability of the system. Internal targets are housed within the system console (as part of a calibration port) and are automatically measured prior to each patient scan. The null target consists of a high optical density glass that returns negligible fluorescence and diffuse reflectance signal when illuminated by the probe. The nominal 10% diffuse reflectance target consists of a flat gray target modified to also contain a central 3.5-mm -diam plastic fluorescent plug and four peripheral phosphorescent plugs. The fluorescence and phosphorescent plugs are used for video and scan mirror alignment. In addition, the intensity of the fluorescence plug is monitored prior to each system use to ensure that the intensity is within predetermined reference values. The signal from the nominal 10% reflectance target is used in the diffuse reflectance calibration procedure (see next) and corrects for changes in the broadband source over time. The frequency double Nd:YAG laser is used to account for temperature drifts observed in the spectrometer.

### 2.3 *Wavelength Calibration*

The CCD spectral bins 11 to 401 are converted to wavelength by use of fundamental reference lines from mercury and argon pen lamps (models 6035 and 6033, Oriel Instruments, Stratford, Connecticut). Individual bins are converted to wavelengths using a fourth-order polynomial fit to the measured bin position of five mercury lines (365.01, 404.66, 435.84, 546.08, and 578.05 nm) and two argon lines (696.54 and 738.40 nm). In this way, wavelength calibration between 360 and 720 nm is determined to within ±1 nm. Wavelength accuracy is also checked and corrected prior to each patient scan by use of the 532-nm line from the focusing and alignment laser. If the measured value is within 3 nm of the expected value, the wavelength axis of the data is shifted to correspond to the measured laser line; if the deviation exceeds 3 nm, the scan is aborted and recalibration would be required. Systematic run-time wavelength drifts of ±1.5 nm from full system calibration were observed in a small number of spectrometers (2 of 16) due to 10°C temperature differences that occurred, depending on how long the system was turned on. Manufacturing changes to the grating mounts alleviated this dependency.

### 2.4 *Fluorescence Signal Calibration*

The fluorescence signal from tissue is calibrated using a multistep procedure requiring 1. calibration data recorded at the time of full system calibration, and 2. calibration data recorded just prior to tissue measurements. The combined calibration elements are shown in Eq. (1) for each interrogation location $i$, and at wavelength $\lambda$.

$$F_C(i,\lambda) = \left\{ \frac{F(i,\lambda) - B_F(i,\lambda)}{E_F(i)} - \left\langle \frac{N(i,\lambda) - B_N(i,\lambda)}{E_N(i)} \right\rangle_i \right\} \cdot \left\{ \frac{\dfrac{L(i,\lambda_n) - B_L(i,\lambda_n)}{W(\lambda_n,T) \times \lambda_n}}{\dfrac{L(i,\lambda) - B_L(i,\lambda)}{W(\lambda,T) \times \lambda}} \cdot \frac{\dfrac{D_c}{176} \times (879\ \text{cts}/\mu\text{J} - \text{nm})}{\dfrac{D(i,\lambda_{\max}) - B_D(i,\lambda_{\max})}{E_D(i)} - \left\langle \dfrac{N(i,\lambda) - B_N(i,\lambda)}{E_N(i)} \right\rangle_i} \right\}_{\text{Cal}} . \quad (1)$$

The terms in the first bracket correspond to tissue and calibration data measured during the patient visit, while the terms in the second bracket correspond to stored calibration data made at the last full system calibration. The following terms have units of detector counts, which are proportional to the optical intensity: the fluorescence signal from tissue ($F$), the back-

ground signal accounting for detector background and external stray light ($B$), the relative measured energy from the laser ($E$), the null-target signal accounting for internal stray light ($N$), the signal from a calibrated blackbody lamp ($L$), and the fluorescence signal from a fluorescence dye standard ($D$). The bracket $\langle \ldots \rangle_i$ implies an average of the null-target signal over the 499 measurement sites. The null-target is housed in the calibration port and is measured just prior to patient or dye-cell measurements, and accounts for any slight differences in internal stray light due to variations in individual probe sheath windows. The relative per pulse energy from the laser is measured by integrating the signal recorded in bins 402 to 522 after subtracting the background signal.

The spectral sensitivity of the system is found by dividing the calibrated lamp signal $L$ by the calibration spectral irradiance values $W$ at each wavelength. The spectral sensitivity is divided by $\lambda$ to convert from watts to number of photons, then normalized to unity at $\lambda_n = 500$ nm. Planck's radiation law for a blackbody emitter (at reference temperature $T$) is used to interpolate the spectral irradiance values measured at discrete wavelengths to the array of wavelengths at each detector bin.

The fluorescence signals from all systems are calibrated relative to a fluorescence dye standard ($1.2 \times 10^{-5}$ M Coumarin 515 in ethylene glycol). The peak of the dye fluorescence ($\lambda_{max}$) is observed around 490 nm when dissolved in ethylene glycol. The term $D_c$ corresponds to the peak fluorescence intensity of the dye at 337-nm excitation divided by the reference peak of the water O-H stretch Raman vibration ($\sim 3350\ \mathrm{cm}^{-1}$), which controls for calibration across dye lots. The value 176 corresponds to the ratio of the dye fluorescence peak to water Raman peak for the progenitor solution, which yielded an average of 879 counts/($\mu$J-nm) measured on the first ten systems. Following calibration, fluorescence emission is reported in absolute units of counts/nm-$\mu$J.

### 2.5 *Diffuse Reflectance Signal Calibration*

The reflectance signal from tissue is also calibrated using a multistep procedure requiring 1. calibration data recorded at the time of full system calibration, and 2. calibration data recorded just prior to tissue measurements. The combined calibration elements are shown in Eq. (2) for each interrogation location $i$, and at wavelength $\lambda$.

$$R_C(i,\lambda) = \left\{ \frac{\dfrac{R(i,\lambda) - B_R(i,\lambda)}{E_R(i)} - \left\langle \dfrac{N(i,\lambda) - B_N(i,\lambda)}{E_N(i)} \right\rangle_i}{\left\langle \dfrac{C(i,\lambda) - B_C(i,\lambda)}{E_C(i)} - \dfrac{N(i,\lambda) - B_N(i,\lambda)}{E_N(i)} \right\rangle_k} \right\} \cdot \left\{ \frac{\left\langle \dfrac{C(i,\lambda) - B_C(i,\lambda)}{E_C(i)} - \dfrac{N(i,\lambda) - B_N(i,\lambda)}{E_N(i)} \right\rangle_k}{\dfrac{R_{60}(i,\lambda) - B_{R_{60}}(i,\lambda)}{E_{R_{60}}(i)} - \left\langle \dfrac{N(i,\lambda) - B_N(i,\lambda)}{E_N(i)} \right\rangle_i} \right\}_{\mathrm{cal}} \cdot T_{60}(\lambda). \qquad (2)$$

Here, $R$ and $R_{60}$ refer to the diffuse reflectance signal from tissue and from a calibrated 60% diffuse reflectance target (SRS-60-010, Labsphere, Sutton, New Hampshire), respectively. The terms in the first bracket correspond to tissue and calibration data measured during the patient visit, while the terms in the second bracket correspond to stored calibration data established at the last full system calibration. The quantity $T_{60}$ corresponds to the calibrated values from the 60% reference target. The following terms have units of detector counts that are proportional to the optical intensity: the reflectance signals from tissue ($R$) and the 60% diffuse reflectance target ($R_{60}$), the background signal accounting for detector background and external stray light ($B$), the relative measured energy from the flashlamp ($E$), the null-target signal accounting for internal stray light ($N$), and the reflectance signal from a 10% diffuse reflectance target ($C$). The bracket $\langle \ldots \rangle_i$ implies an average over the 499 measurement sites. The null target is housed in the calibration port and is measured just prior to patient, or dye-cell, measurements, and accounts for any slight difference in internal stray light due to variations in individual probe sheath windows.

The 60% diffuse reflectance target is measured during full system calibration procedures. The term $C$ corresponds to a 10% diffuse reflectance target housed in the calibration port and is measured prior to patient measurements (first term) and the 60% target (second term) that is measured at the most recent full system calibration. The 10% target has four phosphorescent spots that are used for aligning the scan mirror relative to a defined optical axis, and a central fluorescence spot that is used as a calibration check. As a result, only a portion of this target is available for diffuse reflectance measurements precluding its use as the calibrated reflectance standard. The bracket $\langle \ldots \rangle_k$ implies an average of the 10% diffuse reflectance target over the 499 measurement sites, minus the sites covered by the phosphorescence and fluorescence targets. The mean 10% diffuse reflectance target is measured before each patient measurement and allows for corrections for changes in the light sources since the most recent maintenance procedure. As before, the diffuse reflectance signals are corrected for electronic background and external stray light $B$, and internal stray light as measured by the null-target signal $N$.

Following calibration, fluorescence and diffuse reflectance spectra are smoothed using a five-point median filter[10] followed by a cubic 27-point Savitzky-Golay filter.[11,12] Following smoothing, the fluorescence and diffuse reflectance spectra are linearly interpolated to 1-nm bins between 360 and 720 nm.

### 2.6 *Spectral Arbitration*

At each scan interrogation location, one fluorescence spectrum and two diffuse reflectance spectra (illuminated with the

upper and lower light sources) are available following spectral calibration. These reflectance spectra are occasionally subject to specular reflections (glare) or vignetting from the speculum (shadows). The reflectance spectra are evaluated for the presence of these effects by comparing differences in shape between spectra recorded with the upper and lower light sources. Specular reflection denoted as mirror-like reflection carries just the illumination spectral response absent tissue influence. As a result glare spectra are more intense and near constant lacking hemoglobin absorption bands, making them easy to distinguish. Diffuse reflectance spectra recorded when a portion of the illumination source is blocked by the speculum blade or vaginal wall tends to be lower when compared to the spectrum recorded with the other illumination source.

Glare in the diffuse reflectance spectra taken with each pair of light sources is identified using the intensities of the reflectance measurements in the 370- to 710-nm spectral range. These two sets of measurements are also compared to evaluate the consistency of the measurements, with anomalous values being indicative of unwanted glare artifact or optical vignetting of one or both of the signals. Diffuse reflectance spectra determined to be affected by either specular reflection or vignetting are rejected. In cases where both spectra are free of such effects, the two spectra are averaged into a single spectrum. Additional treatment for glare missed by spectral arbitration is accomplished with an image processing module.

Fluorescence and reflectance spectra may also have abnormally low signals due to the measurement being made on blood, the os, or a speculum blade. Fluorescence signals at 479 nm and reflectance signals at 499 nm less than predetermined reference values are used to identify spectra having abnormally low signals. Tissue measurement sites having insufficient signal in either the fluorescence spectrum or both diffuse reflectance spectra are excluded from further consideration. Thus, combining the specular reflection, vignetting, and low signal metrics, the spectral arbitration process produces either no spectra, one fluorescence spectrum only, or one fluorescence and one diffuse reflectance spectrum from each measurement site.[13]

### 2.7 *Video Camera and Alignment and Focusing Systems*

Prior to fluorescence and reflectance measurements, a color video camera (GP-KS462HM, Panasonic, Secaucus, New Jersey) captures an image of the cervix for analysis. Broadband light from both flashlamps is used to capture this image. The central optical axis of the video and the spectral channels are equivalent, as the two share most of the probe collection optics. Live video from the camera is also used to focus the ODS onto the cervix using a pattern generated by the alignment and focus laser source. An image of this pattern is captured to verify proper focusing prior to patient scans. Video images of the cervix are also captured once every second during scanning to detect movement of the cervix. Image capture is accomplished with a standard framegrabber board. Video images are captured by stepping the galvonometrically controlled scan mirror to the video position, which directs a view of the cervix toward the video camera collection optics (see Fig 2).

The alignment and focusing system is composed of a 10-mW doubled Nd:YAG laser source (model LCM-T-11ccs, Power Technology Incorporated, Little Rock, Arkansas), four fibers that are bundled together at the input end and have projection optics mounted to their output ends, and optics to couple the laser output into the fiber bundle. The laser output to tissue is designed to be less than 400 $\mu$W at 532 nm.

Probe focus is determined using live video and the four projected green-laser spots arranged at the vertices of a rectangle centered on the cervix. These spots are generated by four illuminators positioned around the probe head at a relatively large angle with respect to the optical axis of the system. The spots move closer to the center of the image as the probe is pushed forward, and away from the center as the probe is pulled back. The probe position is adjusted until the four targeting spots are within four fixed circular targets overlaid on the video image of the cervix. Focus is validated by measuring the position of the spots and comparing them to a pre-established calibration curve that translates distance to probe location.

### 2.8 *Motion Tracking*

Detection of translational motion of the cervix is accomplished with the aid of video images taken once every second during the course of the optical scan. The last one-second segment scan data is reacquired if the distance between the new and last image is more than 0.55 mm. The entire cervix is rescanned if the collective motion over the entire scan is greater than 2.5 mm.

The motion-tracking algorithm is based on the cross-correlation between the gradients of two consecutive images in the scan sequence.[14] The cross-correlation $c(k,l)$ from the gradient images $I_1$ and $I_2$ is given by

$$c(k,l) = \sum_i \sum_j \mathbf{I}_1(i,j)\mathbf{I}_2(i-k,j-l), \tag{3}$$

for displacements $k$ and $l$ in the $x$ and $y$ directions, respectively, where $i$ and $j$ are pixel coordinates. For any image pair, a motion vector is always calculated, even if large nontranslational motion (local deformation, warping, rotation, etc.) exists. Therefore, a sensitive motion validation scheme was implemented that rejects scans with any significant nontranslational motion. For motion model validation, the second image is shifted using the motion vector computed by the motion tracker, and the normalized correlation coefficient $c'(m,n)$ is then calculated for each of 16 validation regions arranged in a $4\times4$ matrix at the center of the image:

$$c'(m,n) = \frac{\sum\sum \mathbf{I}_1(i,j)\cdot\mathbf{I}_2(i,j)}{\left[\sum\sum \mathbf{I}_1^2(i,j)\right]^{1/2}\left[\sum\sum \mathbf{I}_2^2(i,j)\right]^{1/2}}, \tag{4}$$

where $(m,n)$ are region coordinates and the summations are performed over the pixel coordinates $i,j$. The detection of more than three regions with a normalized correlation coefficient of less than 0.35 aborts the scan (invalid motion tracking model).

## 3 Results

### 3.1 *Patient Scan Data*

ODS use on 2271 patients enrolled in evaluation studies was analyzed to assess clinical functionality and reliability of the system. Performance factors included the number of scans required for a result, the effectiveness of a single application of acetic acid, and the total optical exposure in use. Spectral data were evaluated to assess optical performance in clinical patients, including minimum spectral bandwidths required and signal-to-noise performance.

Repeat ODS scans may be necessary as a result of excessive patient motion, failure of the system to report a useful final result, or for an abort by the user for any reason. Of the 2271 patients studied, 96.7% (2197) required only a single full scan, while another 2.9% (65) had two scans, and 0.4% (9) had three or more scans. The reason for rescans was predominantly excessive motion, with the exception of seven cases that were for other reasons. Rescans include those due to partial rescans (due to motion $>0.55$ mm or an optical power level outside of nominal values) and full rescans due to grossly excessive motion or a manual user abort.

The system prompts the user to apply acetic acid to the cervix and allows a scan to commence if it starts within 30 to 120 s after the application. Of the 2271 patients evaluated, 92.1% (2092) required only a single acetic acid application. The most common reasons for reapplication of acetic acid were due to difficulties focusing and aligning the probe prior to scanning. The elapsed time between when acetic acid was applied and the start of a scan was 73.5 s on average with a range between 31 and 123 s. Overall, the mean scan time was 11.9 s, and was less than 15 s in 99% of all cases. After a scan was completed, it took approximately 15 s for a final display result to be shown. Therefore, the total time from application of acetic acid to the display of a final result was typically about 2 min.

### 3.2 *Tissue Optical Exposures*

The optical energy of the system was analyzed and found to be significantly below recognized standards for safe tissue exposure. Optical energy can come from one of three sources: the UV nitrogen laser, the frequency doubled Nd:YAG alignment laser (green), and the broadband xenon lamps. The spectral irradiance of the xenon broadband sources was measured with a calibrated spectroradiometer. The output was found to be relatively flat over the specified 360- to 720-nm spectral window, dropping rapidly below 360 nm to negligible levels at 320 nm and below. The system also has a built-in timer that does not allow the broadband sources to be on for more than 10 min per procedure, thereby strictly limiting optical exposure.

The system does not deliver more than 10 UV laser pulses to any one area of the cervix, again for safety reasons. A value of 35 $\mu$J (mean plus six standard deviations) is used as the worse case single pulse exposure. Using these data and following American Conference of Governmental and Industrial Hygienists (ACGIH) guidelines,[15] the maximum UV exposure to tissue for the system was determined to be 70 times less than the threshold limiting value (Table 1), even when considering the additional UV exposure delivered to tissue from a standard colposcope (OPMI-1FC, Carl Zeiss). The UV output of the OPMI-1FC was significantly lower than previously reported for Leisegang colposcopes.[16] The OPMI-1FC transmits light to the cervix through a fiber optic bundle that effectively filters out light below 370 nm. The Leisegang colposcope directly illuminates the cervix using small diameter, thin lenses and delivers more UV light to the cervix. Optical testing determined that the ODS as used is a class 1 laser product, meaning that the laser output from the system from both the UV and green lasers is safe under any normal use circumstance.

### 3.3 *Aggregate Spectral Files*

Aggregate diffuse reflectance and fluorescence spectra of relatively pure cervical histologic classes, and other colposcopically identified groups, were compiled as a result of a pilot study.[9] Five tissue classes were histologically diagnosed (normal squamous epithelium, normal columnar, metaplasia, CIN 1, and CIN 2,3), and one class was formed by colposcopic impression (normal squamous by impression). Seven additional classes representing obstructions were also identified. The number of patients and spectra in each class are listed in Table 2. These data were used to evaluate the functional performance of the optical system.

### 3.4 *Spectral Arbitration*

The results of spectral arbitration on the 13 aggregate groups are also given in Table 2. As designed, the number of spectra lost due to arbitration is relatively low for the tissue aggregate groups and relatively high for the obstruction groups. The low signal metric captures 2469 of the 3212 sites (77%) recorded on the blades of a metal speculum. A good fraction of blood (72%) and fluids (26%) are filtered by the low signal metric. In the glare group, all 2095 sites have glare in the reflectance data when recorded with the upper or lower light sources, yet only 302 sites (14%) are lost due to glare occurring simultaneously in both spectra. Closer to 50% of the sites would have been lost due to glare had a single light source been used. Cervical edges typically denote the transition between the lower speculum blade and cervical tissue, and, as expected, this group has a higher incidence of vignetting in the reflectance spectra taken with the lower light source. A majority of these sites, however, are preserved due to measurements taken with the upper light source. In a typical scan, both diffuse reflectance spectra from a given site are excluded in less than 5% of the 499 sites measured per cervix.

The results of spectral arbitration can be seen visually in Fig. 3, where the output of arbitration is depicted graphically alongside the color image of the cervix. In this extreme case, 173 of 499 sites were affected by glare or shadowing of the illumination sources, yet data were only lost from four sites in total (four sites had glare in both channels, zero sites had shadow in both channels, and zero sites had combined glare and shadow).

### 3.5 *Signal and Signal to Noise*

Following calibration, fluorescence emission is reported in absolute units of counts/nm-$\mu$J and diffuse reflectance is reported as a percentage relative to light reflected from a calibrated diffuse reflectance target. The pilot study optical detection systems had an average UV laser energy at tissue of

**Table 1** UV optical exposure for optical detection system using worst case exposure conditions and comparison to the threshold limiting value (TLV). Analysis is based on the American Conference of Governmental and Industrial Hygienist (ACGIH) guidelines.[15] The safety ratio is calculated based on a TLV of 3000 $\mu$J/cm$^2$. The spectral radiant UV exposure of UV laser result at 32,000 was measured at 337 nm.

| | Spectral radiant UV exposure ($\mu$J/cm$^2$-nm) | | | | Effective radiant UV exposure for 5-nm bins ($\mu$J/cm$^2$) | | | |
|---|---|---|---|---|---|---|---|---|
| Wavelength (nm) | Xenon source (10 min exposure, two lamps) | Colposcope (10 min exposure) | UV laser (10 scans) | ACGIH effectiveness spectrum | Xenon source (10 min exposure, two lamps) | Colposcope (10 min exposure) | UV laser (10 scans) | All sources |
| 300 | 4.9 | | | 0.30 | 7.3 | | | 7.3 |
| 305 | 4.7 | | | 0.060 | 1.4 | | | 1.4 |
| 310 | 3.5 | | | 0.015 | 0.26 | | | 0.26 |
| 315 | 4.9 | | | 0.0030 | 0.073 | | | 0.073 |
| 320 | 6.7 | | | 0.0010 | 0.033 | | | 0.033 |
| 325 | 25 | | | 0.00050 | 0.064 | | | 0.064 |
| 330 | 110 | | | 0.00041 | 0.22 | | | 0.22 |
| 335 | 360 | <0.2 | 32,000 | 0.00034 | 0.62 | | 11 | 11 |
| 340 | 690 | | | 0.00028 | 0.96 | | | 0.96 |
| 345 | 1400 | | | 0.00024 | 1.6 | | | 1.6 |
| 350 | 1800 | | | 0.00020 | 1.8 | | | 1.8 |
| 355 | 2600 | | | 0.00016 | 2.0 | | | 2.0 |
| 360 | 3800 | | | 0.00013 | 2.5 | | | 2.5 |
| 365 | 3900 | | | 0.00011 | 2.1 | | | 2.1 |
| 370 | 3800 | | | 0.000093 | 1.8 | | | 1.8 |
| 375 | 4400 | 0.41 | | 0.000077 | 1.7 | 0.00016 | | 1.7 |
| 380 | 5000 | 55 | | 0.000064 | 1.6 | 0.018 | | 1.6 |
| 385 | 5900 | 150 | | 0.000053 | 1.6 | 0.039 | | 1.6 |
| 390 | 6300 | 380 | | 0.000044 | 1.4 | 0.083 | | 1.5 |
| 395 | 7700 | 640 | | 0.000036 | 1.4 | 0.11 | | 1.5 |
| 400 | 7100 | 920 | | 0.000030 | 1.1 | 0.14 | | 1.2 |
| | | | | Effective radiant UV exposure ($\mu$J/cm$^2$) | 31 | 0.39 | 11 | 43 |
| | | | | **Safety ratio** | 96 | 7637 | 276 | 70 |

22±3 $\mu$J/pulse, an average photoelectron conversion factor of 10.2±0.4 photoelectrons per count, and a typical quantum efficiency of 0.755 at 500 nm. Combining these values yields a factor of 297 that can be used to approximate counts detected/($\mu$J-nm) to photons detected/nm.

The inherent spectral resolution of the spectrograph, including its 200-$\mu$m input fiber, is 8.3 nm. In subsequent data processing, a Savitzky-Golay smoothing filter produces an effective spectral resolution of 15.6 nm as determined by measuring the full-width at half maximum (FWHM) of a narrow

**Table 2** Aggregate groups and results of spectral arbitration. Column three shows reflectance spectra affected by glare *G*, or vignetting *V*, when illuminated with the upper 1 or lower 2 light sources. Column four shows measurement sites lost due to low fluorescence or reflectance signals (*LS*), glare from both upper and lower light sources (*GG*), glare from the upper and vignetting from the lower light sources (*GV*), vignetting from the upper and glare from the lower light sources (*VG*), and vignetting from both light sources (*VV*).

| | | Number of | | Spectra affected | | | | Spectra lost | | | | | Total |
|---|---|---|---|---|---|---|---|---|---|---|---|---|---|
| Class | Group | patients | spectra | *G*1 | *G*2 | *V*1 | *V*2 | *LS* | *GG* | *GV* | *VG* | *VV* | spectra lost |
| Tissue | CIN 2,3 | 64 | 473 | 10 | 12 | 50 | 16 | 2 | 3 | 0 | 0 | 0 | 5 |
| | CIN 1 | 46 | 226 | 7 | 10 | 3 | 1 | 0 | 0 | 0 | 0 | 0 | 0 |
| | Metaplasia | 78 | 347 | 10 | 16 | 5 | 14 | 5 | 2 | 0 | 0 | 0 | 7 |
| | Normal columnar | 56 | 230 | 10 | 8 | 27 | 15 | 9 | 1 | 0 | 1 | 0 | 10 |
| | Normal squamous | 71 | 297 | 15 | 16 | 5 | 11 | 0 | 2 | 0 | 0 | 0 | 2 |
| | Normal squamous (by impr.) | 56 | 2016 | 31 | 21 | 123 | 34 | 0 | 5 | 0 | 0 | 0 | 5 |
| Obstruction | Glare | 171 | 2095 | 1096 | 1016 | 4 | 33 | 4 | 302 | 8 | 1 | 0 | 315 |
| | Mucus | 119 | 2429 | 81 | 80 | 57 | 357 | 85 | 21 | 9 | 0 | 0 | 113 |
| | Blood | 14 | 175 | 11 | 36 | 28 | 87 | 126 | 1 | 7 | 6 | 2 | 131 |
| | Vaginal wall | 116 | 4965 | 93 | 151 | 639 | 978 | 985 | 19 | 10 | 26 | 0 | 1005 |
| | Fluids | 127 | 2420 | 191 | 21 | 76 | 989 | 638 | 8 | 47 | 0 | 0 | 681 |
| | Cervical edge | 146 | 3401 | 44 | 55 | 295 | 1256 | 255 | 0 | 8 | 18 | 1 | 263 |
| | Metal speculum | 62 | 3212 | 100 | 275 | 1041 | 1566 | 2469 | 12 | 14 | 225 | 0 | 2469 |

reference band (data not shown). The bandwidth of the digital filter was selected based on tissue spectral properties and on the output from the classification algorithm. Typical fluorescence and diffuse reflectance spectra from clinical measurements subsequently identified as CIN 2,3 and normal squamous cervical tissue are shown with and without smoothing in Fig. 4. It is observed that the high frequency noise seen in the unsmoothed data is effectively removed by the digital filters without introducing any distortion to the spectral line shapes. The smoothing routine occurs as one of the last steps in the calibration procedure and is done with the final calibrated spectra. No filtering is performed on the individual calibration spectra, raw tissue, or background spectra. The performance of the classification algorithm did not change for data measured with this system for bandwidths up to 27 points (data not shown).

The signal-to-noise ratios for the spectra were generally very high. Signal-to-noise ratios exceeding 100 were typical over most of the wavelength range for both diffuse reflectance and fluorescence spectra after smoothing. For typical signals from tissue, the signal-to-noise ratios for diffuse reflectance spectra were generally higher than the fluorescence spectra due to the higher signals collected in the reflectance channel.

### 3.6 *System Validation*

The fluorescence and diffuse reflectance spectra were recorded from known standards in ten systems to assess the variability among systems and the deviation from reference values. Ten percent diffuse reflectance targets were used to validate the diffuse reflectance channel [Fig. 5(a)]. The mean(SD) diffuse reflectance signal measured at 500 nm for the ten systems was 9.5%(0.4%) corresponding to a 3.8% variation among systems and a −5% relative deviation from the expected 10% value. The fluorescence dye cells were used to validate the fluorescence channel [Fig. 5(b)]. The mean(SD) fluorescence signal was 871(37) counts/$\mu$J-nm, corresponding to a variation among systems of 4.2% and a relative deviation from the expected value of −0.9%.

Wavelength validation was determined by monitoring the position of the Coumarin-515 peak position. The mean(SD) peak position was 489.9(0.7) nm (range 489 to 491 nm). In addition, the position of 1-nm narrow spectral bands selected between 360 and 720 nm from a commercial spectrophotometer were measured with three systems, and all bands were found to be within ±1 nm from the known output wavelength.

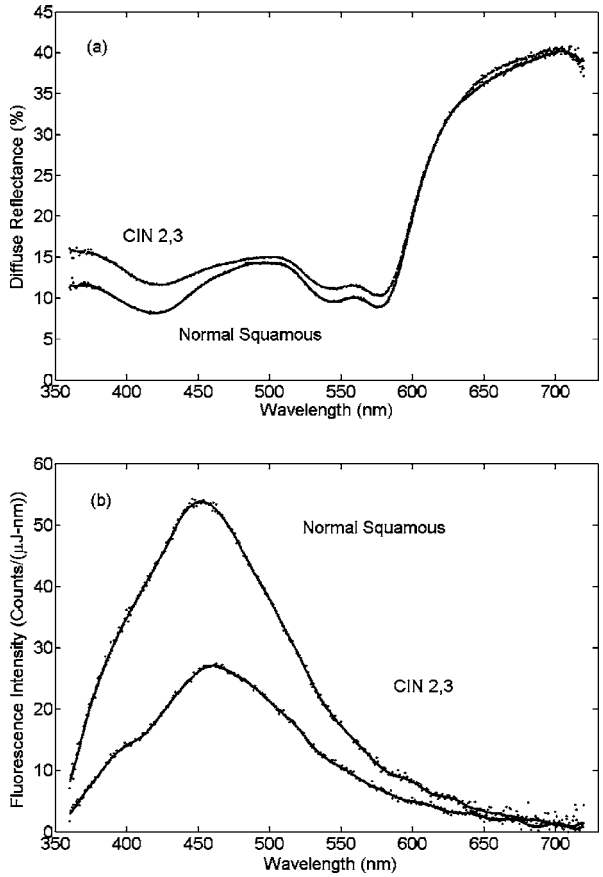


**Fig. 4** Typical (*a*) diffuse reflectance and (*b*) fluorescence spectra of cervical tissue following application of acetic acid. Individual points represent the data before Savitzky-Golay smoothing.

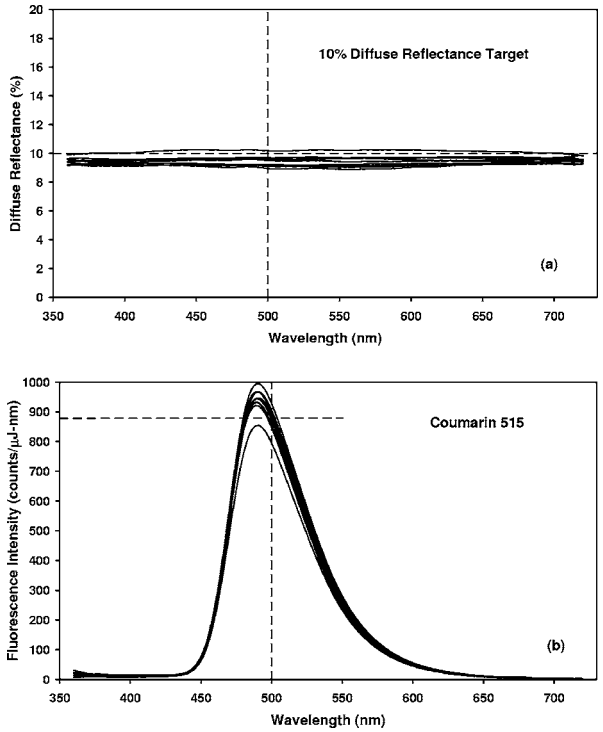


**Fig. 5** Standard (*a*) diffuse reflectance target and (*b*) fluorescence dye spectra as measured on ten calibrated pivotal study systems. The intersection of the dashed lines depicts the true value.

## 4 Discussion

Quantitative optical spectroscopy has been shown to be feasible in identifying cervical intraepithelial neoplasia and is maturing to a point where the commercialization of the technology is possible.[9,17–30] To be practical, robustly calibrated systems are required to minimize variation among systems so that the performance of the system is not device dependent. As a target, the variation among systems should be considerably less than the variability among patients, which have been reported for fluorescence to be around 500% among patients and 25% within any one patient.[31] The current system as described introduces variability on the order of 5%, which is certainly sufficient considering the large patient variability.

The system design and calibration procedures implemented for the optical system reported here are quite comprehensive and account for background signals due to both internal and external stray light. Many designs are used to minimize internal stray light, including antireflective coatings, low fluorescence materials, and the use of baffles and apertures to minimize stray light. The system further accounts for source fluctuations by monitoring the pulse energy on the xenon lamps and the UV laser. All four channels, diffuse reflectance and fluorescence intensity, the video signal, and wavelength, are calibrated to reference standards designed to minimize differences among systems. In all of these ways, the accuracy of the spectral measurements has been shown to be within 5% of target values across multiple systems in clinical use.

Diffuse reflectance measurements in tissue are commonly made with optical probes designed to avoid specular reflections by placing the probe in contact with tissue. The current system includes a novel means of illuminating the tissue that allows diffuse reflectance to be measured from tissue remotely. In general, if specular reflection is noted in one of the illumination channels, it is not noted in the second. When evaluating spectra collected from sites that had glare observed visually, only 14% of the sites (302 of 2095) had glare noted in both channels (Table 2). In a single patient scan, no more than 5 of the 499 interrogation points (1%) are lost because glare is present in both channels. On average, 1.8 points (302/171) are lost due to glare.

The current system was not designed to correct for variations in spectral response that could occur between full calibration procedures. In addition to the use of high quality optics that are robust to changes over time, additional run-time optical checks such as drops in the system throughput or an increase in the internal stray light are monitored to account for optics that become dirty over time. Review of calibration data on more than 2000 clinical patients over a one-year period demonstrated that the calibration deviations were within expected and acceptable levels. The only significant change observed was that below 400 nm, and was attributed to aging of the single-use optical sheath. This change is inherently compensated for in the diffuse reflectance channel, and the classification algorithm employed does not use fluorescence data below 400 nm.

The fluorescence intensities reported here can be compared to other optical detection systems by multiplying the counts/$\mu$J-nm units reported here by a factor of 297 to convert to photons detected/nm. The collection efficiency of the system is estimated to be $8.5\times10^{-4}$, assuming tissue to be a 4-pi isotropic emitter. Overall optical throughput is estimated to be about 0.072, accounting for transmission losses through all optical elements. Using a method described previously, the fluorescence efficiency for normal squamous and CIN 2,3 tissues are estimated to be $1.0\times10^{-3}$ and $5.4\times10^{-4}$, respectively, for 337-nm excitation, which is four to five times less than the values reported previously in the literature.[32]

The cervical imaging system was designed to find CIN 2,3 with the aid of contrast gained through the application of acetic acid to the cervix, a common technique practiced by colposcopists. Acetic acid increases scattering, especially from the nuclei of neoplastic tissue.[33–36] As a result, diffuse reflectance signal from CIN 2,3 is generally higher than other nonneoplastic tissues.[37] In addition, the fluorescence signal decreases,[37] presumably due to increased nuclear scattering. Changes in pH may also account for some of the difference seen in the fluorescence signal, as the fluorescence from normal tissue also decreases. Diffuse reflectance and fluorescence systems that do not use acetic acid typically present lower signals from neoplastic tissue, primarily due to increased hemoglobin and structural changes in tissue.[24,38] Earlier system designs measured the cervix before and at various times after applying acetic acid. From this work, it was found that a single scan made between 30 and 130 s after the application of acetic acid was optimal.[39]

In summary, a noncontact optical detection system was developed for the *in vivo* detection of high-grade cervical intraepithelial neoplasia (CIN 2,3). Diagnostic scans of the entire cervix were performed following acetic acid application using laser-induced fluorescence spectroscopy, white light diffuse reflectance spectroscopy, and video imaging. A typical cervical scan took 12 s to complete, and a typical procedure time was about 2 min. Diffuse reflectance and fluorescence spectra with signal-to-noise ratios better than 100-to-1 were collected between 360 and 720 nm. Glare reduction and optical vignetting in the diffuse reflectance data were handled with a novel illumination scheme with subsequent spectral arbitration. Typical accuracies and variance among systems were found to be acceptable at 5% following normal use calibration.

## Acknowledgment

The authors wish to acknowledge Perry Banks, Mike Oradnik, Harry Gao, John Flanagan, Rolf Saager, and Alex Zelenchuk for their contributions toward the development of the optical detection system. Funding for this study was provided by MediSpectra, Incorporated.

## References

1. T. C. Wright, Jr., J. T. Cox, L. S. Massad, J. Carlson, L. B. Twiggs, and E. J. Wilkinson, "2001 consensus guidelines for the management of women with cervical intraepithelial neoplasia," *Am. J. Obstet. Gynecol.* **189**, 295–304 (2003).
2. J. T. Cox, M. Schiffman, and D. Solomon, "Prospective follow-up suggests similar risk of subsequent cervical intraepithelial neoplasia grade 2 or 3 among women with cervical intraepithelial neoplasia grade 1 or negative colposcopy and directed biopsy," *Am. J. Obstet. Gynecol.* **188**, 1406–1412 (2003).
3. ALTS Study Group, "Results of a randomized trial on the management of cytology interpretations of atypical squamous cells of undetermined significance," *Am. J. Obstet. Gynecol.* **188**, 1383–1392 (2003).
4. ALTS Study Group, "A randomized trial on the management of low-grade squamous intraepithelial lesion cytology interpretations," *Am. J. Obstet. Gynecol.* **188**, 1393–1400 (2003).
5. R. A. Drezek, R. Richards-Kortum, M. A. Brewer, M. S. Feld, C. Pitris, A. Ferenczy, M. L. Faupel, and M. Follen, "Optical imaging of the cervix," *Cancer* **98**, 2015–2027 (2003).
6. N. Ramanujam, "Fluorescence spectroscopy of neoplastic and non-neoplastic tissues," *Neoplasia* **2**, 89–117 (2000).
7. R. Richards-Kortum and E. Sevick-Muraca, "Quantitative optical spectroscopy for tissue diagnosis," *Annu. Rev. Phys. Chem.* **47**, 555–606 (1996).
8. K. Sokolov, M. Follen, and R. Richards-Kortum, "Optical spectroscopy for detection of neoplasia," *Curr. Opin. Chem. Biol.* **6**, 651–658 (2002).
9. W. K. Huh, R. M. Cestero, F. A. Garcia, M. A. Gold, R. S. Guido, K. McIntyre-Seltman, D. M. Harper, L. Burke, S. T. Sum, R. F. Flewelling, and R. D. Alvarez, "Optical detection of high-grade cervical intraepithelial neoplasia in vivo: results of a 604-patient study," *Am. J. Obstet. Gynecol.* **190**, 1249–1257 (2004).
10. W. K. Pratt, *Digital Image Processing*, pp. 330–333, John Wiley and Sons, New York (1978).
11. S. J. Orfanidis, "Signal processing applications," Chap. 8 in *Introduction to Signal Processing*, Prentice-Hall, Englewood Cliffs, NJ (1996).
12. A. Savitzky and M. J. E. Golay, "Smoothing and differentiation of data by simplified least squares procedures," *Anal. Chem.* **36**, 1627–1639 (1964).
13. K. T. Schomacker, T. Meese, M. Ouradnik, J. Flanagan, and H. Gao, "Method and apparatus for identifying spectral artifacts," U.S. 6,818,903, MediSpectra (2004).
14. J. P. Lewis, "Fast normalized cross-correlation," in *Vision Interface*, pp. 120–123 (1995).
15. "Ultraviolet radiation," in *Documentation of the Threshold Limit Values for Physical Agents, American Conference of Governmental and Industrial Hygienists* (2001).
16. C. K. Brookner, A. Agrawal, E. V. Trujillo, M. F. Mitchell, and R. R. Richards-Kortum, "Safety analysis: relative risks of ultraviolet exposure from fluorescence spectroscopy and colposcopy are comparable," *Photochem. Photobiol.* **65**, 1020–1025 (1997).
17. J. M. Benevides, S. Shang, S. Y. Park, and R. Richards-Kortum, "Multispectral digital colposcopy for in vivo detection of cervical cancer," *Opt. Express* **11**, 1223–1236 (2003).
18. L. Burke, M. Modell, J. Niloff, M. Kobelin, G. Abu-Jawdeh, and A. Zelenchuk,"Identification of squamous intraepithelial lesions: Fluorescence of cervical tissue during colposcopy," *J. Lower Genital Tract Dis.* **3**, 159–162 (1999).
19. S. K. Chang, M. Follen, A. Malpica, U. Utzinger, G. Staerkel, D. Cox, E. N. Atkinson, C. MacAulay, and R. Richards-Kortum, "Optimal excitation wavelengths for discrimination of cervical neoplasia," *IEEE Trans. Biomed. Eng.* **49**, 1102–1111 (2002).
20. S. K. Chang, Y. N. Mirabal, E. N. Atkinson, D. Cox, A. Malpica, M. Follen, and R. Richards-Kortum, "Combined reflectance and fluorescence spectroscopy for in vivo detection of cervical pre-cancer," *J. Biomed. Opt.* **10**, 024031 (2005).
21. D. G. Ferris, R. A. Lawhead, E. D. Dickman, N. Holtzapple, J. A. Miller, S. Grogan, S. Bambot, A. Agrawal, and M. L. Faupel, "Multimodal hyperspectral imaging for the noninvasive diagnosis of cervical neoplasia," *J. Lower Genital Tract Dis.* **5**, 65–72 (2001).
22. I. Georgakoudi, B. C. Jacobson, M. G. Muller, E. E. Sheets, K. Badizadegan, D. L. Carr-Locke, C. P. Crum, C. W. Boone, R. R. Dasari, J. Van Dam, and M. S. Feld, "NAD(P)H and collagen as in vivo quantitative fluorescent biomarkers of epithelial precancerous changes," *Cancer Res.* **62**, 682–687 (2002).
23. A. Mahadevan, M. F. Mitchell, E. Silva, S. Thomsen, and R. R. Richards-Kortum, "Study of the fluorescence properties of normal and neoplastic human cervical tissue," *Lasers Surg. Med.*, **13**, 647–655 (1993).
24. Y. N. Mirabal, S. K. Chang, E. N. Atkinson, A. Malpica, M. Follen, and R. Richards-Kortum, "Reflectance spectroscopy for in vivo detection of cervical precancer," *J. Biomed. Opt.* **7**, 587–594 (2002).

25. A. Nath, K. Rivoire, S. Chang, L. West, S. B. Cantor, K. Basen-Engquist, K. Adler-Storthz, D. D. Cox, E. N. Atkinson, G. Staerkel, C. MacAulay, R. Richards-Kortum, and M. Follen, "A pilot study for a screening trial of cervical fluorescence spectroscopy," *Int. J. Gynecol. Cancer* **14**, 1097–1107 (2004).
26. R. J. Nordstrom, L. Burke, J. M. Niloff, and J. F. Myrtle, "Identification of cervical intraepithelial neoplasia (CIN) using UV-excited fluorescence and diffuse-reflectance tissue spectroscopy," *Lasers Surg. Med.* **29**, 118–127 (2001).
27. N. Ramanujam, M. F. Mitchell, A. Mahadevan, S. Thomsen, A. Malpica, T. Wright, N. Atkinson, and R. Richards-Kortum, "Spectroscopic diagnosis of cervical intraepithelial neoplasia (CIN) in vivo using laser-induced fluorescence spectra at multiple excitation wavelengths," *Lasers Surg. Med.* **19**, 63–74 (1996).
28. N. Ramanujam, M. F. Mitchell, A. Mahadevan, S. Thomsen, A. Malpica, T. Wright, N. Atkinson, and R. Richards-Kortum, "Development of a multivariate statistical algorithm to analyze human cervical tissue fluorescence spectra acquired *in vivo*," *Lasers Surg. Med.* **19**, 46–62 (1996).
29. N. Ramanujam, M. F. Mitchell, A. Mahadevan-Jansen, S. L. Thomsen, G. Staerkel, A. Malpica, T. Wright, N. Atkinson, and R. Richards-Kortum, "Cervical precancer detection using a multivariate statistical algorithm based on laser-induced fluorescence spectra at multiple excitation wavelengths," *Photochem. Photobiol.* **64**, 720–735 (1996).
30. A. Milbourne, S. Y. Park, J. L. Benedet, D. Miller, T. Ehlen, H. Rhodes, A. Malpica, J. Matisic, D. Van Niekirk, E. N. Atkinson, N. Hadad, N. Mackinnon, C. Macaulay, R. Richards-Kortum, and M. Follen, "Results of a pilot study of multispectral digital colposcopy for the in vivo detection of cervical intraepithelial neoplasia," *Gynecol. Oncol.* **99**, S67–75 (2005).
31. C. Brookner, U. Utzinger, M. Follen, R. Richards-Kortum, D. Cox, and E. N. Atkinson, "Effects of biographical variables on cervical fluorescence emission spectra," *J. Biomed. Opt.* **8**(3), 479–483 (2003).
32. E. V. Trujillo, D. Sandison, U. Utzinger, N. Ramanujam, M. F. Mitchell, and R. Richards-Kortum, "Method to determine tissue fluorescence efficiency in vivo and predict signal-to-noise ratios of spectroscopy," *Appl. Spectrosc.* **52**, 943–951 (1998).
33. R. Lambert, J. F. Rey, and R. Sankaranarayanan, "Magnification and chromoscopy with the acetic acid test," *Endoscopy* **35**, 437–445 (2003).
34. M. Rajadhyaksha, S. Gonzalez, and J. M. Zavislan, "Detectability of contrast agents for confocal reflectance imaging of skin and microcirculation," *J. Biomed. Opt.* **9**(2), 323–331 (2004).
35. K. Sokolov, R. Drezek, K. Gossage, and R. Richards-Kortum, "Reflectance spectroscopy with polarized light: is it sensitive to cellular and nuclear morphology," *Opt. Express* **5**, 302–317 (1999).
36. A. F. Zuluaga, R. Drezek, T. Collier, R. Lotan, M. Follen, and R. Richards-Kortum, "Contrast agents for confocal microscopy: how simple chemicals affect confocal images of normal and cancer cells in suspension," *J. Biomed. Opt.* **7**(3), 398–403 (2002).
37. A. Agrawal, U. Utzinger, C. Brookner, C. Pitris, M. F. Mitchell, and R. Richards-Kortum, "Fluorescence spectroscopy of the cervix: influence of acetic acid, cervical mucus, and vaginal medications," *Lasers Surg. Med.* **25**, 237–249 (1999).
38. U. Utzinger and R. R. Richards-Kortum, "Fiber optic probes for biomedical optical spectroscopy," *J. Biomed. Opt.* **8**(1), 121–147 (2003).
39. K. T. Schomacker, A. Zelenchuk, R. Flewelling, and H. Kaufman, "Optimal windows for obtaining optical data for characterization of tissue samples," U.S. 6,933,154, MediSpectra, Inc. (2005).